The structure of phospholamban pentamer reveals a channel-like architecture in membranes

Kirill Oxenoid and James J. Chou*

Department of Biological Chemistry and Molecular Pharmacology, Harvard Medical School, Boston, MA 02115

Communicated by Stephen C. Harrison, Harvard Medical School, Boston, MA, June 14, 2005 (received for review May 10, 2005)

Contraction and relaxation of heart muscle cells is regulated by cycling of calcium between cytoplasm and sarcoplasmic reticulum. Human phospholamban (PLN), expressed in the sarcoplasmic reticulum membrane as a 30-kDa homopentamer, controls cellular calcium levels by a mechanism that depends on its phosphorylation. Since PLN was discovered ≈30 years ago, extensive studies have aimed to explain how it influences calcium pumps and to determine whether it acts as an ion channel. We have determined by solution NMR methods the atomic resolution structure of an unphosphorylated PLN pentamer in dodecylphosphocholine micelles. The unusual bellflower-like assembly is held together by leucine/isoleucine zipper motifs along the membrane-spanning helices. The structure reveals a channel-forming architecture that could allow passage of small ions. The central pore gradually widens toward the cytoplasmic end as the transmembrane helices twist around each other and bend outward. The dynamic N-terminal amphipathic helices point away from the membrane, perhaps facilitating recognition and inhibition of the calcium pump.

leucine/isoleucine zipper | membrane channel | NMR | dipolar couplings

Phospholamban (PLN) in the sarcoplasmic reticulum (SR) membrane of cardiomyocytes regulates the level of intracellular calcium, the main determinant of muscle contraction and relaxation. In the unphosphorylated form, PLN has an inhibitory effect on the sarco(endo)plasmic reticulum calcium ATPase (SERCA), a membrane protein responsible for pumping most of the calcium from the cytoplasm into the SR, thereby causing relaxation of myofibrils. Heart stimulants, such as adrenaline, set off a chain of signal transduction events that among other effects lead to PLN phosphorylation. Phosphorylated PLN no longer inhibits SERCA, allowing for more efficient pumping of calcium. Imbalance in the PLN–SERCA interaction leads to deterioration of heart function and cardiomyopathy (1). *In vitro* experiments have suggested that SERCA binds PLN by stripping a subunit away from the unphosphorylated 30-kDa pentamer, thereby depolymerizing PLN assembly (2, 3), but the nature of this interaction is still not understood. In addition to its role as a calcium pump regulator, there have been early ion conductance studies suggesting that PLN is also an ion channel (4). This hypothesis has not been tested further due in part to the lack of structural information on the PLN pentamer.

To elucidate a potential dual function of PLN, we have determined the structure of the unphosphorylated human PLN pentamer by solution NMR methods at 30°C and compared it with that of a monomeric mutant (5). The pentamer structure reveals a number of previously undescribed features. The unusual axial orientation and flexibility of the extramembrane helices in the pentamer may facilitate recognition by SERCA, whereas the supercoiling and bending of the membrane-spanning helices leads to formation of a funnel-like channel with a hydrophobic neck, as in many known ion channels.

Methods

Protein Preparation. The gene encoding wild-type human PLN was cloned into the pMALc2x vector (New England Biolabs) and expressed as a maltose-binding protein (MBP) fusion protein. Cells were lysed by sonication, and the lysate was passed through an amylose resin that specifically binds MBP. The pure MBP–PLN fusion protein was eluted from the resin by maltose. PLN was released from MBP by cleavage by tobacco etch virus protease and subsequently was purified to homogeneity by HPLC using a C18 reverse-phase column. The PLN pentamer was reconstituted by first dissolving PLN in solution containing 25 mM sodium phosphate (pH 6.0), 6 M guanidine·HCl, 50 mM β-mercaptoethanol, and 200 mM dodecylphosphocholine (DPC) and subsequently removing the denaturant by dialysis.

NMR Spectroscopy. All NMR experiments were conducted on spectrometers (Bruker, Billerica, MA) at 30°C. Complete sequence-specific assignment of backbone $^{1}H^{N}$, ^{15}N, $^{13}C^{\alpha}$, $^{13}C^{\beta}$, $^{13}C'$, and side-chain methyl resonances are described in *Supporting Methods* and also Fig. 6, which are published as supporting information on the PNAS web site. For measurements of $^{3}J_{C'C\gamma}$ and $^{3}J_{NC\gamma}$ coupling constants for determining side-chain χ_1 rotamers for residues other than Thr, Val, and Ile, quantitative-*J* approaches based on the ^{1}H-^{15}N constant-time heteronuclear single-quantum coherence were used (6, 7). For couplings involving ^{15}N, a transverse relaxation-optimized spectroscopy version of the experiments were carried out at 750 MHz, whereas experiments for coupling involving C′ were performed at 500 MHz. For $^{3}J_{C'C\gamma}$ and $^{3}J_{NC\gamma}$ of Thr, Val, and Ile, and $^{3}J_{C\alpha C\delta}$ (used to derive the χ_2 rotamers) of Leu and Ile, 2D spin-echo difference methods based on ^{1}H-^{13}C constant-time heteronuclear single-quantum coherence were used (8–10). These spectra were recorded at 600 MHz. All three-bond couplings are given in Table 2, which is published as supporting information on the PNAS web site.

For residual dipolar coupling (RDC) measurements, weak alignment of the DPC-reconstituted PLN was accomplished by using a modified version (11) of the strain-induced alignment in a gel method (12) (see *Supporting Methods* for more details). Three types of backbone RDCs, $^{1}D_{NH}$, $^{1}D_{C'C\alpha}$, and $^{1}D_{C'N}$, were measured by using 3D HNCO type experiments. The ^{1}H-^{15}N couplings were measured at 600 MHz (^{1}H frequency) by interleaving the 3D HNCO experiments (13), with and without ^{1}H CPD decoupling (14), both acquired with 50 ms of mixed-CT ^{15}N evolution. The $^{13}C'$-$^{13}C^{\alpha}$ couplings were obtained at 500 MHz from the standard 3D HNCO recorded with 80 ms of $^{13}C^{\alpha}$-coupled $^{13}C'$ evolution. The one-bond $^{13}C'$-N couplings were measured at 600 MHz by using the 3D transverse relaxation-optimized spectroscopy–HNCO in a quantitative-*J* manner (15). Based on the length of the time domain data and the signal-to-noise ratio (14), the accuracy of the measured RDCs is expected to be at ±0.5 Hz ($^{1}D_{NH}$), ±0.5 Hz ($^{1}D_{C'C\alpha}$), and ±0.3 Hz ($^{1}D_{NC'}$).

Intramonomer nuclear Overhauser effects (NOEs) were assigned by using two 3D ^{15}N-edited NOESY spectra recorded with

Abbreviations: AP, amphipathic ; DPC, dodecylphosphocholine; NOE, nuclear Overhauser effect; PLN, phospholamban; RDC, residual dipolar coupling; SERCA, sarco(endo)plasmic reticulum calcium ATPase; SR, sarcoplasmic reticulum; TM, transmembrane.

Data deposition: The structure of the PLN pentamer has been deposited to the Protein Data Bank, www.pdb.org (PDB ID code 1ZLL).

*To whom correspondence should be addressed. E-mail: james_chou@hms.harvard.edu.

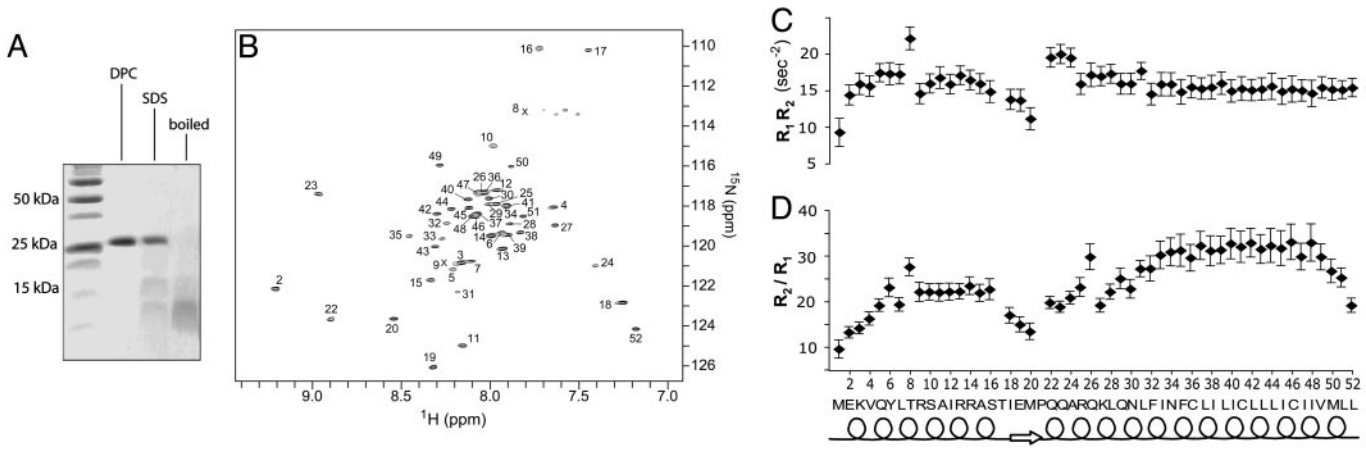

Fig. 1. NMR characterization of PLN pentamer. (*A*) SDS/PAGE of PLN reconstituted in 200 mM DPC and SDS under reducing conditions. Lane 1 shows the molecular mass marker. In lanes 2 and 3, PLN was reconstituted in DPC and SDS, respectively, and was loaded on the gel without boiling. For lane 4, the DPC-reconstituted sample was boiled for 30 min before loading and pentamers were disrupted. The PLN concentration (0.02 mM) is the same in lanes 2–4. (*B*) A 750-MHz ^{1}H-^{15}N transverse relaxation-optimized spectroscopy spectrum of 0.2 mM PLN pentamer in DPC. Each peak represents a backbone NH moiety with residue number labeled. The C5 rotational symmetry is manifested in the presence of one set of 50 amide peaks. (*C*) The products of ^{15}N longitudinal (R_1) and transverse (R_2) relaxation rates used to probe variations in chemical exchange (26); the rates were recorded at ^{1}H frequency of 600 MHz by using experiments that closely followed that of Farrow *et al.* (45). (*D*) The different ratios of R_2 to R_1 for AP and TM helices indicate that the AP helices are mobile relative to the TM helices in the pentamer.

NOE mixing of 80 and 120 ms and two 3D ^{13}C-edited NOESY spectra recorded with 120- and 160-ms mixing times. NOEs between adjacent monomers in the pentamer were assigned by a combined analysis of 3D ^{15}N-edited, double-^{13}C-filtered NOESY of a mixed sample and standard 3D ^{13}C-edited NOESY of a homogeneous ^{15}N,^{13}C-labeled sample. For the carbon-filtered NOESY experiment, a mixed sample consisting of 0.5 mM ^{15}N,^{13}C-labeled PLN and 0.5 mM unlabeled PLN was prepared. The 3D ^{15}N-edited, double-^{13}C-filtered NOESY (200 ms NOE mixing) that incorporates two carbon filters (16) was used to suppress NOEs between amide protons of the labeled subunit and ^{13}C-attached aliphatic protons. This method allowed exclusive observation of NOEs between the amide protons of labeled subunits and protons of unlabeled subunits. Because we were specifically targeting amide-methyl NOEs, filtering delays were optimized to completely purge the ^{13}C-attached methyl protons. As a negative control, the same filtered NOESY experiment was recorded for a 1 mM ^{15}N,^{13}C-labeled protein sample with half the number of transients used for the mixed protein sample. Additionally, the intermonomer NOEs were observed by using a simple ^{15}N-edited NOESY recorded with 300 ms NOE mixing on a sample consisting of 0.5 mM ^{15}N-labeled, 100% ^{2}H-labeled PLN and 0.5 mM unlabeled PLN (17).

Structure Calculation. All structure calculations were performed by using the program X-PLOR-NIH (18). For monomer structure determination, a standard high-temperature simulated annealing protocol (19) was first used to calculate the structure from a random coil by using intramonomer NOEs, backbone dihedral restraints derived from chemical shifts (20), and side-chain χ_1/χ_2 restraints as shown in Table 2. The converged structure subsequently was refined by RDCs for residues 2–51 by using a low-temperature simulated annealing protocol (21–23) in the presence of all other restraints. The following describes the details of such refinement. For the helical region (residues 3–15 and 23–51), O–H^{N} and O–N hydrogen bond distance restraints of 2 and 3 Å were enforced with flat-well (±0.2 Å) harmonic potentials, with the force constant fixed at 20 kcal·mol^{-1}·Å^{-2}. Intramonomer NOE restraints also were enforced by flat-well harmonic potentials, with the force constant fixed at 50 kcal·mol^{-1}·Å^{-2}. For side-chain χ_1 and χ_2 angles that are not

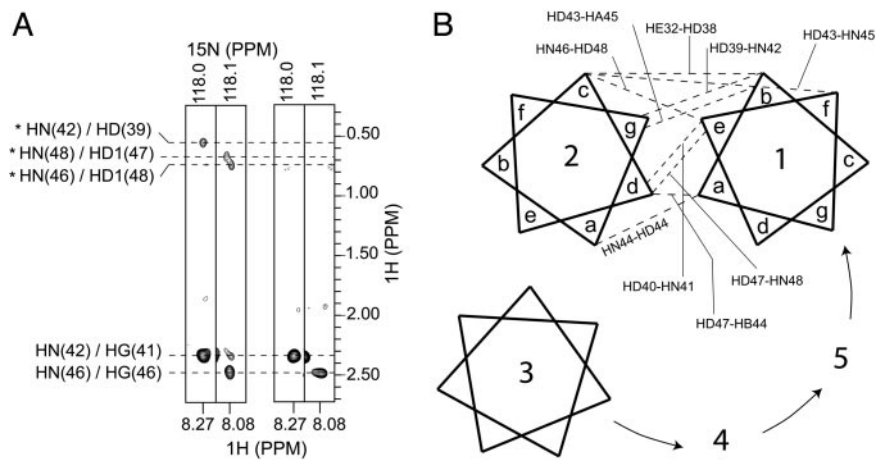

Fig. 2. Intermonomer distance restraints. (*A*) Strips from the 3D ^{15}N-edited, double-^{13}C-filtered NOESY experiment (16) that was optimized to exclusively observe NOEs between the amide protons of ^{15}N,^{13}C-labeled subunits and protons not covalently attached to ^{13}C atoms, particularly those of methyl groups. Intermonomer NOEs were unambiguously identified when the experiment was performed on a mixed sample reconstituted with a 1:1 ratio of ^{15}N,^{13}C-labeled and unlabeled subunits (two left strips). As a negative control (two right strips), the same experiment was recorded for a pure ^{15}N,^{13}C-labeled sample with measurement time scaled to match the spectral intensity of the mixed sample. The three intermonomer NOEs shown here (labeled with stars) correspond respectively to (HN42^{i}, HD39^{i+1}), (HN 48^{i}, HD47^{i+1}), and (HN46^{i}, HD48^{i-1}) proton pairs, where the monomer index (*i*) increases in the counterclockwise direction as in *B*. The two strong NOEs near 2.4 ppm are intramonomer NOEs to the HS of C41 and C46. They are observed because HS of Cys is not attached to ^{13}C. (*B*) Heptad repeat diagram illustrating nine unambiguous intermolecular NOEs (dashed lines) between adjacent subunits. The lengths of the dashed lines do not reflect relative interproton distances.

assigned as rotamer averaging in Table 2, flat-well (±30°) harmonic potentials were applied with force constant fixed at 30 kcal·mol^{-1}−rad^{-2}. Finally, RDC restraint force constant is ramped from 0.0005 to 0.15 kcal·mol^{-1}·Hz^{-2} (normalized for the $^1D_{NH}$ couplings). Other force constants, commonly used in NMR structure calculation, are: k(vdw) = 0.002 → 4.0 kcal·mol^{-1}·Å^{-2}, k(impr) = 0.1 → 1.0 kcal·mol^{-1}·degree^{-2}, and k(bond angle) = 0.4 → 1.0 kcal·mol^{-1}·degree^{-2}. During the annealing run, the bath was cooled from 300 to 20 K with a temperature step of 10 K. A total of 20 monomer structures were calculated by using this protocol. The lowest-energy structure was chosen as the average monomer structure for subsequent pentamer assembly.

To determine the average pentamer structure, five copies of the lowest-energy subunit structure calculated above were used. The C$^\alpha$ atoms of residues 2–51 of each monomer were grouped and treated as rigid body, while the side chains were permitted to rotate. This calculation was performed in X-PLOR by using the "dynamics internal" option (18). A high-temperature simulated annealing then was performed in the absence of RDC restraints and in the presence of intermonomer NOEs and other intramonomer restraints. Here, for each experimental intermonomer NOE between two adjacent subunits, five identical distance restraints were assigned respectively to all pairs of neighboring subunits to satisfy the condition of rotational symmetry. These restraints were enforced by flat-well (±1.0 Å) harmonic potentials, with the force constant ramped from 10 to 50 kcal·mol^{-1}·Å^{-2}. During the annealing run, the bath was cooled from 2,000 to 200 K with a temperature step of 20 K.

Results and Discussion

NMR Characterization of the Symmetric Pentamer. For NMR studies, the PLN pentamer was reconstituted in 25 mM sodium phosphate (pH 6.0), 50 mM β-mercaptoethanol, and 200 mM DPC to a final concentration of 1 mM monomer (0.2 mM pentamer). DPC has previously been shown to be a suitable detergent for oligomeric membrane protein reconstitution and structural studies by solution NMR (24). A high concentration of β-mercaptoethanol was used to prevent nonspecific disulfide linkage, because the pentameric assembly contains a total of 15 Cys residues. The reconstituted PLN in DPC was shown by gel electrophoresis to be a pentamer (Fig. 1*A*), in agreement with similar experiments reported in the literature (25). Together with the results in Fig. 1*A*, the high-resolution ^{1}H-^{15}N correlation spectrum in Fig. 1*B* shows that in the above sample condition, PLN assembles homogeneously into well-structured pentamers with fivefold rotational symmetry. The absence of large chemical exchange broadening in the transmembrane (TM) region (residues 25–52), as probed by the product of ^{15}N longitudinal (R_1) and transverse (R_2) relaxation rates (26) (Fig. 1*C*), reflects the stability of the pentamer, because transient association and dissociation of subunits would introduce substantial line-broadening of NMR resonances. The sizable variations in the ratios of ^{15}N R_2 to R_1 indicate the presence of significant internal dynamics (27) between N- and C-terminal segments of the protein (Fig. 1*D*).

Owing to the symmetric, parallel packing proposed for the TM segments of PLN (28), intermonomer distances of <5 Å are mostly between methyl groups belonging to either the same or vicinal positions in the polypeptide chain, making unambiguous assignment of intermonomer NOEs very difficult. To circumvent the problem, we used a two-stage divide-and-conquer strategy, consisting of (*i*) overdetermination of the subunit structure by a large number of structural restraints and (*ii*) rigid-body assembly of subunits into the pentamer with a modest number of intermonomer NOE restraints. The monomer structure was determined with an X-PLOR simulated annealing protocol that refined against 193 intramonomer distance restraints derived from NOEs, 115 backbone orientation restraints derived from RDCs, and 53 side-chain χ_1/χ_2 restraints derived from 97 three-bond J couplings. Precise definition of the equivalent subunits greatly reduced the degrees of freedom of the system, thereby allowing accurate determination of the pentameric structure with nine intermonomer NOEs (Fig. 2; see also Table 3, which is published as supporting information on the PNAS web site) or, equivalently, 45 intermonomer distance restraints for the symmetric pentamer. To assemble the pentamer, the backbones of the individual monomers (residues 2–51) were treated as rigid bodies while the side chains were allowed to move relative to each other (see *Methods* for details). The average pentamer structure then was determined by satisfying all intramonomer and intermonomer NOEs and side-chain J couplings. An ensemble of 30 pentamer structures was calculated, and the statistics of the 20 lowest-energy structures are presented in Table 1. The precision of the average pentamer structure is shown in Fig. 3*A*. Additionally, to estimate the uncertainty in the orientation of the extramembrane helix relative to the TM helix as described only by NOEs in the context of the pentamer, the same simulated annealing protocol was used while treating the backbones of

Table 1. NMR and refinement statistics

Statistic	PLN pentamer
NMR distance and dipolar and dihedral constraints*	
Distance constraints	
Intramonomer	965
Intermonomer	45
Hydrogen bonds	350
Backbone RDC contraints†	
NH	43
C′Cα	31
NC′	41
Total dihedral angle restraints	
χ_1	175
χ_2	90
Structure statistics	
Violations (mean and SD)	
Distance constraints, Å	0.088 ± 0.001
Dihedral angles constraints	3.720 ± 0.237
RDCs, rms in Hz‡	2.5 (2–15); 2.4 (23–51); 3.9 (2–51)
Max. dihedral angle violation, °	3.980
Max. distance constraint violation, Å	0.089
Deviations from idealized geometry	
Bonds, Å	0.0039 (0.000004)
Angles, °	0.583 (0.023)
Impropers, °	0.656 (0.010)
ϕ/ψ in most favored or allowed region, %§	98
Average pairwise rms deviation, Å	
Backbone	0.61
Heavy	1.10

Statistics are calculated and averaged over 20 lowest-energy pentamer structures, obtained from a total of 30 calculated structures. The precision of the atomic coordinates is defined as the average rms differences between the 20 structures and their mean coordinates.

*The numbers of experimental constraints shown here, except RDCs, are summed over all five subunits.

†Since RDCs were only used for the refinement of individual subunits, the number of RDC constraints shown here are for each subunit.

‡The rms difference between experimental dipolar couplings and those predicted by refined structures (averaged over 20 structures) by means of singular value decomposition fit. All couplings are normalized to $^1D_{NH}$. Due to the mobility of AP helix relative to the TM helix, no single conformer of the subunit can satisfy all RDCs simultaneously. Therefore, rms values of fittings are shown separately for regions 2–15 and 23–51.

§The program PROCHECK NMR (50) is used to assess the quality of calculated structures.

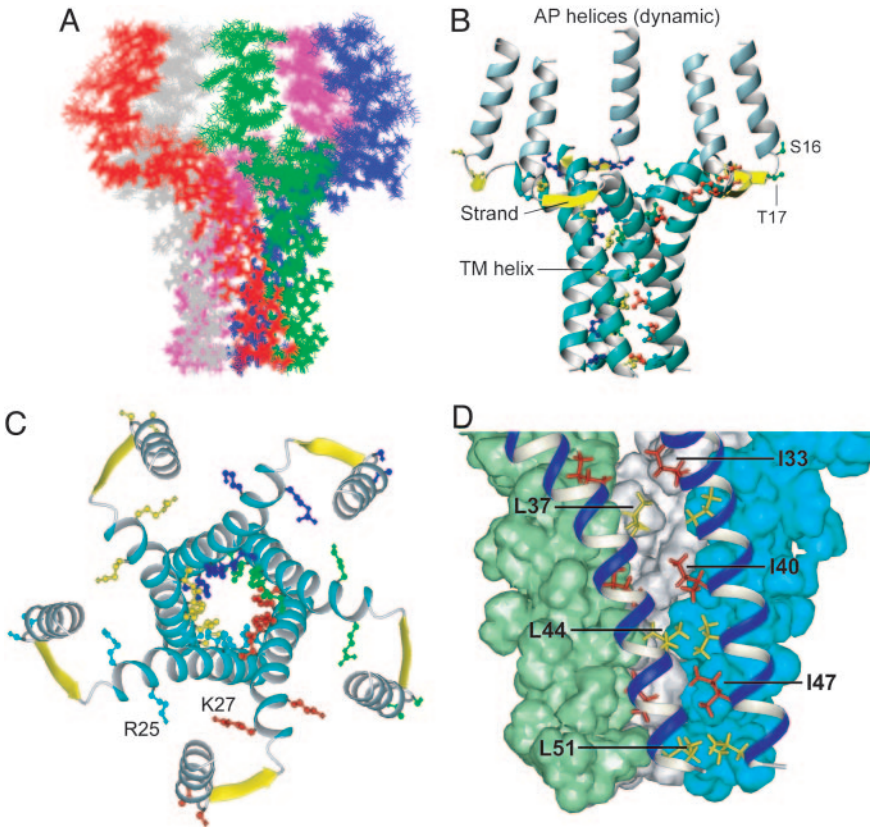

Fig. 3. Overall structure of the PLN pentamer. (*A*) Average rms differences between 20 lowest energy structures and their mean (0.61 Å for backbone and 1.1 Å for heavy atoms). (*B* and *C*) Ribbon representations of the side and top view of the pentamer structure, respectively. The yellow strands shown here do not represent β-strands; they are used to emphasize that residues 18–20 have backbone dihedral angles similar to that of β-strands. The side chains of important residues are shown in different colors for different subunits, including those involved in the zipper interaction, the positively charged R25 and K27 that may be important for keeping the adjacent TM helices away from each other at the N terminus, as well as the phosphorylation sites of S16 and T17 next to the hinge joining the AP helix and the strand. Protons are not displayed here for clarity. (*D*) A close-up view of residues (labeled) involved in the Leu/Ile zipper interaction, as well as the tight van der Waals packing between neighboring subunits. Pictures were generated by using the program MOLMOL (46).

residues 23–51 as rigid bodies. The structure ensemble is shown in Fig. 7, which is published as supporting information on the PNAS web site.

Structure of PLN Pentamer. As shown in Fig. 3 *B* and *C*, each subunit consists of a short, positively charged amphipathic (AP) α-helix (residues 2–15), an extended linker (residues 16–22) in which residues 18–20 acquire dihedral angles characteristic of β-strand, and a long, largely hydrophobic TM α-helix (residues 23–52). Although NMR relaxation rates report higher-than-average internal dynamics for the linker (Fig. 1*D*), it is mostly structured, as indicated by the presence of large dipolar couplings and medium-range NOEs.

The pentamer is held together by Leu/Ile zipper interactions involving side chains of the C-terminal portion (residues 37–51) of the TM helices (Fig. 3*D*), consistent with prior mutagenesis data and a proposed model of "zipper" interactions (25, 28). The Leu residues at position "*a*" of a heptad repeat (Fig. 2*B*), L37, L44, and L51, form three inner hydrophobic rings, while the Ile residues at position "*d*", I40 and I47, fill in the space between the Leu rings. The structure suggests that I33 is partially involved in the packing as well. As in the case of the TM region of the glycophorin A dimer (29), PLN pentameric assembly maximizes the van der Waals interaction surface, an important feature of stable and specific association of monomers in a membrane environment. Moreover, it is apparent from the structure that to optimize van der Waals fit, adjacent helices cross at an angle of $\approx$19° with a left-handed twist. It has been demonstrated by packing energy minimization calculations that left-handed twisting of a helix bundle is usually energetically favorable (30).

The overall topology of the individual subunits is similar to that of the AFA-PLN (PLN with C36A, C41F, and C46A mutations) monomeric mutant, which adopts an L-shaped conformation in DPC micelles (5) (see Fig. 8 *A* and *B*, which is published as supporting information on the PNAS web site). A hydrophobic core formed by residues A15, T17, I18, M20, and A24 stabilizes the relative orientation of AP and TM helices (see Fig. 9*C*, which is published as supporting information on the PNAS web site), but the perfect L-shape of the free monomer is considerably distorted in the pentamer. The major difference is that the TM helix is straight in the monomeric mutant but severely bent at the L37 position in the pentamer. RDCs (31) unambiguously identified the bending (Fig. 9), because ^{1}H-^{15}N RDCs fit poorly to a straight helix with Pearson correlation coefficient (r) of 0.65. Additionally, when $^{13}C'$-$^{13}C^{\alpha}$ RDCs were used to validate the degree of bending, they agreed well with the bent TM helix calculated with ^{1}H-^{15}N and $^{13}C'$-^{15}N RDCs (r = 0.96) but not with the straight helical conformation (r = 0.80). The pentamer structure in Fig. 3 offers a plausible explanation for the strong curvature. The monomers are bundled together by zipper interactions between neighboring C-terminal halves (residues 37–52) of the TM helices, with almost no specific packing interactions between N-terminal halves (residues 23–36). Moreover, the N terminus is highly charged at R25 and K27. Thus, electrostatic repulsion can keep the helices away from each other, thereby bending them near L37. The consequences of such bending are a much larger opening at the N terminus of the central

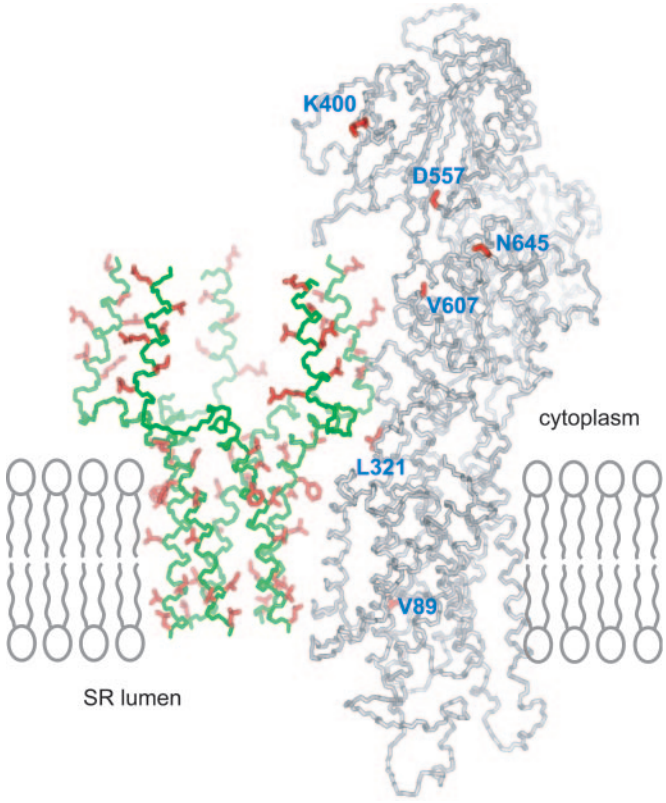

Fig. 4. A model for initial recognition between the PLN pentamer and SERCA. The backbones of PLN and SERCA are colored in green and gray, respectively. PLN residues important for SERCA interaction as indicated by mutagenesis studies are colored in red, including E2, V4, L7, R9, I12, and R14 of the AP helix (34) and L31, N34, F35, I38, L42, I48, V49, and L52 of the TM helix (3). The model of SERCA was derived from that for the E2 form of rabbit SERCA1a (PDB ID code 1IWO); residues from the proposed groove in the extramembrane domain where PLN AP helix bind are shown in red, including K400, D557, V607, and N645.

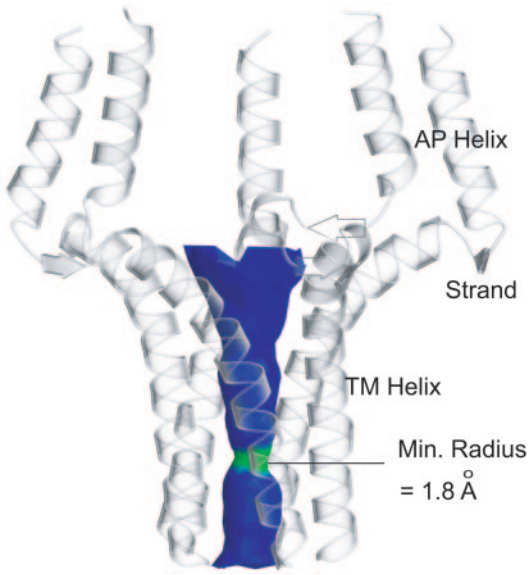

Fig. 5. The pore surface calculated by using the program HOLE (47) and displayed by MOLSCRIPT (48) and RASTER3D (49). The region of the channel colored in green is only wide enough to allow passing of one water molecule, whereas the blue portion can accommodate two or more water molecules.

channel and an axial orientation of the AP helices. The finding that both AP and TM helices are oriented roughly along the presumed bilayer normal is consistent with Fourier transform infrared and CD studies of PLN pentamer in lipid membranes (32). Overall, the PLN pentamer has an unusual bellflower-like architecture that has not been seen before in membrane proteins. It must be emphasized here that the differences in the R_2/R_1 ratios (Fig. 1*D*) show that the AP helix must be partially mobile relative to the TM helix. Hence, the relative orientation shown in Fig. 3 represents only the ensemble average sampled by RDCs and NOEs on the NMR time scale.

Models for PLN–SERCA Interaction. PLN regulates calcium flux across the SR membrane by inhibiting the Ca^{2+}–ATPase SERCA. Monomeric mutants such as AFA–PLN form stable complexes with SERCA and are fully functional in SERCA inhibition (3, 33). It has therefore been proposed that PLN is in a monomer–pentamer equilibrium in the SR membrane and that it is the monomer that interacts with the calcium pump while the pentamer plays a role of monomer storage (1). PLN reconstituted *in vitro* forms very stable pentamers, however, as expected for a supercoiled Leu/Ile zipper. Indeed, DPC-reconstituted PLN runs as a pentamer without chemical crosslinking in SDS/PAGE under reducing condition (Fig. 1*A*) and to some extent even in the presence of 8 M urea (K.O. and J.J.C., unpublished results), consistent with previously reported experiments (25). We could detect no NMR resonances corresponding to monomers (Figs. 1*B* and 6). The tight assembly raises the following question: How available are monomeric PLN for association with SERCA?

The pentamer structure allows us to examine whether the individual subunits in the oligomeric assembly can initiate interaction with the calcium pump. Previous mutagenesis studies have shown that residues in PLN that are important for SERCA interaction do not contribute to pentamer formation (3, 28, 34). These residues are E2, V4, L7, R9, I12, and R14 of the AP helix and L31, N34, F35, I38, L42, I48, V49, and L52 of the TM helix. As shown in Fig. 4, the residues of the TM helix that are important for SERCA interaction are all on the membrane side of the pentamer except for N34 and I48, which are at the interface of neighboring subunits. These residues therefore could interact with the membrane-spanning region of SERCA. Moreover, the relatively mobile AP helix, which on average points away from the presumed membrane surface, could fit into a groove in the SERCA cytoplasmic domain (Fig. 4) that has been proposed based on chemical crosslinking experiments to accommodate the AP helix (35). These structural features suggest that PLN in the pentameric form can initiate binding of SERCA without having to dissociate first. Fig. 4 shows, however, that the original subunit conformation in the pentamer cannot simultaneously satisfy the distance restraints between PLN and SERCA that were derived from chemical crosslinking data, which include distances between K3, N27, and L49 of PLN and K400, L321, and V89 of SERCA, respectively (3, 36). To satisfy these contacts, a PLN subunit may have to be significantly stretched. Therefore, it is possible that PLN pentamer initially recognizes SERCA by forming a transient intermediate complex, and this interaction provides the energy to strip a subunit out of the oligomeric assembly, and the released PLN monomer would then rearrange and form a stable complex with SERCA. This model is consistent with previous *in vitro* experiments, in which the addition of SERCA to wild-type PLN increases the percentage of PLN monomers observed by fluorescence energy transfer experiments (2).

Alternatively, inhibitory interactions with SERCA may take place without the removal of the subunit from the pentamer and therefore at a much lower energetic cost. In this scenario, the AP helix would have to unwind to satisfy the chemical crosslinking data.

The unwinding could be facilitated by the plastic and unstable nature of the AP helix. Indeed, the AP helices are not stabilized by helix–helix contacts in the pentamer, and the fast amide proton exchange for T8 and R9 (Fig. 1*B*) suggests the absence of H-bonds in this part of the helix. This model also leads us to speculate that phosphorylation of PLN could reduce its affinity for the pump. The phosphorylation sites S16 and/or T17 are located next to the joint of the AP helix and the strand (Fig. 3*B*). Introducing negative charges at this region could potentially alter the average orientation of the AP helix so that it is much less accessible to the calcium pump.

PLN Pentamer as a Potential Ion Channel. Ever since the characterization of PLN as a homopentamer in the SR membrane, its function as an ion channel has been a matter of debate (4, 37). The pentamer structure reveals a funnel-like pore of ≈28 Å in length (Fig. 5). Not including C36 and C41, the pore consists entirely of hydrophobic residues involved in the Leu/Ile zipper interactions. The pore opens up in both directions, from its narrowest part, ≈3.6 Å in diameter, at the level of L44 side chains, to 7.8 Å at the N terminus and 5.8 Å at the C terminus. Hydrophobic pores are common in the known structures of gated ion channels, and the most constricted region of the pore usually is ringed by hydrophobic amino acid side chains, such as Leu or Val (38–40). The N-terminal mouth of the pore is rich in Asn, Gln, and positively charged Lys and Arg side chains, whereas the C terminus is hydrophobic. The structure therefore raises the possibility that the PLN pentamer might function as an ion channel.

The pore is not suitable for proton conductance, which requires the formation of a stream of H-bonded water molecules, or "a wire of ice," across the channel. Because the neck of the pore is wide enough to accommodate only one water molecule and no H-bonding groups are in position to coordinate the "wire" formation, a continuous chain of water molecules cannot be established across the PLN pore. Many of the physiologically relevant ions such as Na^+, K^+, Ca^{2+}, and Cl^- are small enough to pass the L44 ring in unhydrated form. The energetic cost for these ions to lose their water shell is large, although the sulfhydryl groups of C36 and C41 near the neck must contribute to offsetting the cost of dehydration.

The possibility of PLN conducting ion is attractive from a physiological point of view. During Ca^{2+} movement across the SR membrane, an equivalent amount of counterions (e.g., the ubiquitous Cl^-) must cross the membrane to maintain electro-neutrality. A number of research groups have measured chloride currents in the SR (41, 42), but a Cl^- channel of the SR membrane is yet to be identified. It is interesting to note in this context that in one chloride conductance study, monoclonal anti-PLN antibody abolished chloride current across the membrane of SR-derived vesicles (43). PLN also has partial structural similarity with the channel-like cartilage oligomeric matrix protein (COMP), an extracellular, water-soluble coiled-coil pentamer. The COMP pentamer forms a long and narrow pore (diameter ≈ 2–6 Å), in which a Cl^- ion was observed (44), suggesting that pores formed by coiled-coil pentamers are capable of accommodating Cl^- ions. Further experiments are needed to test ion channel properties of PLN.

In conclusion, the PLN pentamer has a channel-like architecture. The structure reveals some unexpected features such as the strong curvature of the TM helix and the axial orientation of the AP helix. The AP helix orientation and flexibility make it available for interaction with SERCA. The residues of the TM helix that participate in PLN–SERCA interaction are lipid-exposed in the pentamer and are also accessible to SERCA. Hence, the structure of PLN pentamer is consistent with a possible dual role of PLN as a regulatory protein and as an ion channel. The structure presented here sets the stage for a series of future experiments to characterize the effect of phosphorylation on the orientation and dynamics of the AP helices, as well as the properties of the pore. Our work demonstrates that recent advances in solution NMR technology now enable high-resolution structure determination of small and medium-sized oligomeric membrane channels.

We thank Stephen Harrison and Gerhard Wagner for critical reading of the manuscript. This work was supported by the Smith Family Award for Young Investigators. J.J.C. is a Pew scholar.

1. MacLennan, D. H. & Kranias, E. G. (2003) *Nat. Rev. Mol. Cell. Biol.* **4,** 566–577.
2. Reddy, L. G., Jones, L. R. & Thomas, D. D. (1999) *Biochemistry* **38,** 3954–3962.
3. Kimura, Y., Kurzydlowski, K., Tada, M. & MacLennan, D. H. (1997) *J. Biol. Chem.* **272,** 15061–15064.
4. Kovacs, R. J., Nelson, M. T., Simmerman, H. K. & Jones, L. R. (1988) *J. Biol. Chem.* **263,** 18364–18368.
5. Zamoon, J., Mascioni, A., Thomas, D. D. & Veglia, G. (2003) *Biophys. J.* **85,** 2589–2598.
6. Hu, J.-S., Grzesiek, S. & Bax, A. (1997) *J. Biomol. NMR* **9,** 323–328.
7. Hu, J.-S., Grzesiek, S. & Bax, A. (1997) *J. Am. Chem. Soc.* **119,** 1803–1804.
8. Vuister, G. W., Wang, A. C. & Bax, A. (1993) *J. Am. Chem. Soc.* **115,** 5334–5335.
9. Grzesiek, S., Vuister, G. W. & Bax, A. (1993) *J. Biomol. NMR* **3,** 487–493.
10. MacKenzie, K. R., Prestegard, J. H. & Engelman, D. M. (1996) *J. Biomol. NMR* **7,** 256–260.
11. Chou, J. J., Gaemers, S., Howder, B., Louis, J. M. & Bax, A. (2001) *J. Biomol. NMR* **21,** 377–382.
12. Tycko, R., Blanco, F. J. & Ishii, Y. (2000) *J. Am. Chem. Soc.* **122,** 9340–9341.
13. Ikura, M., Kay, L. E. & Bax, A. (1990) *Biochemistry* **29,** 4659–4667.
14. Kontaxis, G., Clore, G. & Bax, A. (2000) *J. Magn. Reson.* **143,** 184–196.
15. Chou, J. J., Delaglio, F. & Bax, A. (2000) *J. Biomol. NMR* **18,** 101–105.
16. Zwahlen, C., Legault, P., Vincent, S. J. F., Greenblatt, J., Konrat, R. & Kay, L. E. (1997) *J. Am. Chem. Soc.* **119,** 6711–6721.
17. Walters, K. J., Matsuo, H. & Wagner, G. (1997) *J. Am. Chem. Soc.* **119,** 5958–5959.
18. Schwieters, C. D., Kuszewski, J., Tjandra, N. & Clore, G. M. (2002) *J. Magn. Reson.* **160,** 66–74.
19. Nilges, M., Clore, G. M. & Gronenborn, A. M. (1988) *FEBS Lett.* **239,** 129–136.
20. Cornilescu, G., Delaglio, F. & Bax, A. (1999) *J. Biomol. NMR* **13,** 289–302.
21. Chou, J. J., Li, S. P., Klee, C. B. & Bax, A. (2001) *Nat. Struct. Biol.* **8,** 990–997.
22. Chou, J. J., Li, S. P. & Bax, A. (2000) *J. Biomol. NMR* **18,** 217–227.
23. Chou, J. J., Kaufman, J. D., Stahl, S. J., Wingfield, P. T. & Bax, A. (2002) *J. Am. Chem. Soc.* **124,** 2450–2451.
24. Oxenoid, K., Kim, H. J., Jacob, J., Sonnichsen, F. D. & Sanders, C. R. (2004) *J. Am. Chem. Soc.* **126,** 5048–5049.
25. Karim, C. B., Stamm, J. D., Karim, J., Jones, L. R. & Thomas, D. D. (1998) *Biochemistry* **37,** 12074–12081.
26. Kneller, J. M., Lu, M. & Bracken, C. (2002) *J. Am. Chem. Soc.* **124,** 1852–1853.
27. Kay, L. E., Torchia, D. A. & Bax, A. (1989) *Biochemistry* **28,** 8972–8979.
28. Simmerman, H. K., Kobayashi, Y. M., Autry, J. M. & Jones, L. R. (1996) *J. Biol. Chem.* **271,** 5941–5946.
29. MacKenzie, K. R., Prestegard, J. H. & Engelman, D. M. (1997) *Science* **276,** 131–133.
30. Chou, K. C., Maggiora, G. M., Nemethy, G. & Scheraga, H. A. (1988) *Proc. Natl. Acad. Sci. USA* **85,** 4295–4299.
31. Tjandra, N. & Bax, A. (1997) *Science* **278,** 1111–1114.
32. Arkin, I. T., Rothman, M., Ludlam, C. F., Aimoto, S., Engelman, D. M., Rothschild, K. J. & Smith, S. O. (1995) *J. Mol. Biol.* **248,** 824–834.
33. Mueller, B., Karim, C. B., Negrashov, I. V., Kutchai, H. & Thomas, D. D. (2004) *Biochemistry* **43,** 8754–8765.
34. Toyofuku, T., Kurzydlowski, K., Tada, M. & MacLennan, D. H. (1994) *J. Biol. Chem.* **269,** 3088–3094.
35. Toyoshima, C., Asahi, M., Sugita, Y., Khanna, R., Tsuda, T. & MacLennan, D. H. (2003) *Proc. Natl. Acad. Sci. USA* **100,** 467–472.
36. James, P., Inui, M., Tada, M., Chiesi, M. & Carafoli, E. (1989) *Nature* **342,** 90–92.
37. Arkin, I. T., Adams, P. D., Brunger, A. T., Smith, S. O. & Engelman, D. M. (1997) *Annu. Rev. Biophys. Biomol. Struct.* **26,** 157–179.
38. Zhou, Y., Morais-Cabral, J. H., Kaufman, A. & MacKinnon, R. (2001) *Nature* **414,** 43–48.
39. Bass, R. B., Strop, P., Barclay, M. & Rees, D. C. (2002) *Science* **298,** 1582–1587.
40. Beckstein, O., Biggin, P. C. & Sansom, M. S. (2001) *J. Phys. Chem. B* **105,** 12902–12905.
41. Tanifuji, M., Sokabe, M. & Kasai, M. (1987) *J. Membr. Biol.* **99,** 103–111.
42. Rousseau, E., Roberson, M. & Meissner, G. (1988) *Eur. Biophys. J.* **16,** 143–151.
43. Decrouy, A., Juteau, M., Proteau, S., Teijiera, J. & Rousseau, E. (1996) *J. Mol. Cell. Cardiol.* **28,** 767–780.
44. Malashkevich, V. N., Kammerer, R. A., Efimov, V. P., Schulthess, T. & Engel, J. (1996) *Science* **274,** 761–765.
45. Farrow, N. A., Muhandiram, R., Singer, A. U., Pascal, S. M., Kay, C. M., Gish, G., Shoelson, S. E., Pawson, T., Forman-Kay, J. D. & Kay, L. E. (1994) *Biochemistry* **33,** 5984–6003.
46. Koradi, R., Billeter, M. & Wuthrich, K. (1996) *J. Mol. Graphics* **14,** 51–55.
47. Smart, O. S., Goodfellow, J. M. & Wallace, B. A. (1993) *Biophys. J.* **65,** 2455–2460.
48. Kraulis, P. J. (1991) *J. Appl. Crystallogr.* **24,** 946–950.
49. Merritt, E. A. & Bacon, D. J. (1997) *Methods Enzymol.* **277,** 505–524.
50. Laskowski, R. A., MacArthur, M. W., Moss, D. S. & Thornton, J. W. (1993) *J. Appl. Crystallogr.* **26,** 283–291.